REPORT DOCUMENTATION PAGE

Form Approved
OMB No. 0704-0188

1. AGENCY USE ONLY *(Leave Blank)*	2. REPORT DATE	3. REPORT TYPE AND DATES COVERED
	1/25/99	Final Progress, 9/15/96 - 12/31/98

4. TITLE AND SUBTITLE
Photonic Crystal Flat Panel Radiators for Wideband High Power Antennas

5. FUNDING NUMBERS
DAAH04-96-1-0439

6. AUTHORS
Edl Schamiloglu, Kevin J. Malloy, Kamil Agi, and Mohammad Mojahedi

7. PERFORMING ORGANIZATION NAME(S) AND ADDRESS(ES)
Center for High Technology Materials
University of New Mexico
1313 Goddard SE
Albuquerque, NM 87131

8. PERFORMING ORGANIZATION REPORT NUMBER

9. SPONSORING / MONITORING AGENCY NAME(S) AND ADDRESS(ES)
U.S. Army Research Office
P.O. Box 12211
Research Triangle Park, NC 27709-2211

10. SPONSORING / MONITORING AGENCY REPORT NUMBER
35629-PH-SAH

11. SUPPLEMENTARY NOTES
The views, opinions and/or findings contained in this report are those of the authors and should not be construed as an official Department of the Army position, policy or decision, unless so designated by other documentation.

12a. DISTRIBUTION / AVAILABILITY STATEMENT
Approved for public release; distribution unlimited.

12b. DISTRIBUTION CODE

13. ABSTRACT *(Maximum 200 words)*

This final progress report summarizes the main accomplishments of this program. In particular, we detail the accomplishments during the final funding period, i.e., since the submission of the last interim progress report. The two areas that we focused on in this period were i) the integration of a microstrip patch antenna with a two-dimensional photonic crystal substrate, and ii) the time and frequency domain detection of superluminal group velocity in one-dimensional photonic crystals. For the two-dimensional photonic crystal substrate work, we studied the effects of a finite-sized ground plane on the resonance frequency of a microstrip patch antenna. A finite-difference-time-domain (FDTD) code was used for these studies, and the calculations were found to be in good agreement with the experimental characterizations. The effect of a defect state under the antenna location was also studied and found to improve the performance. For the one-dimensional photonic crystal characterization studies, a transfer matrix technique was used to obtain analytical closed form expressions for both the transmission and reflection coefficients of a plane wave incident onto it. We were able to experimentally measure superluminal group velocities for propagation through the "stop-band" of a one-dimensional photonic crystal. This result is not inconsistent with special relativity or causality since the frontal (forerunner) velocity of the signal never exceeds the speed of light in vacuum. These results are important for a fundamental understanding of electromagnetic wave propagation through short interaction regions with anomalous dispersion.

14. SUBJECT TERMS
photonic crystals, ultra wideband microwaves, superluminality, microstrip patch antenna

15. NUMBER OF PAGES
36

16. PRICE CODE

17. SECURITY CLASSIFICATION OF REPORT	18. SECURITY CLASSIFICATION OF THIS PAGE	19. SECURITY CLASSIFICATION OF ABSTRACT	20. LIMITATION OF ABSTRACT
UNCLASSIFIED	UNCLASSIFIED	UNCLASSIFIED	UL

NSN 7540-01-280-5500

Standard Form 298 (Rev. 2-89)
Prescribed by ANSI Std. Z39-1
298-102

Photonic Crystal Flat Panel Radiators for Wideband High Power Antennas

Final Progress Report

E. Schamiloglu, K.J. Malloy, K. Agi, and M. Mojahedi

January 25, 1999

U.S. Army Research Office

Grant DAAH04-96-1-0439

Center for High Technology Materials
University of New Mexico
1313 Goddard SE
Albuquerque, NM 87131

This final progress report summarizes the main accomplishments of this program. In particular, we detail the accomplishments during the final funding period, i.e., since the submission of the last interim progress report. The two areas that we focused on in this period were i) the integration of a microstrip patch antenna with a two-dimensional photonic crystal substrate, and ii) the time and frequency domain detection of superluminal group velocity in one-dimensional photonic crystals. For the two-dimensional photonic crystal substrate work, we studied the effects of a finite-sized ground plane on the resonance frequency of a microstrip patch antenna. A finite-difference-time-domain (FDTD) code was used for these studies, and the calculations were found to be in good agreement with the experimental characterizations. The effect of a *defect state* under the antenna location was also studied and found to improve the performance. For the one-dimensional photonic crystal characterization studies, a transfer matrix technique was used to obtain analytical closed form expressions for both the transmission and reflection coefficients of a plane wave incident onto it. We were able to experimentally measure superluminal group velocities for propagation through the "stop-band" of a one-dimensional photonic crystal. This result is not inconsistent with special relativity or causality since the frontal (forerunner) velocity of the signal never exceeds the speed of light in vacuum. These results are important for a fundamental understanding of electromagnetic wave propagation through short interaction regions with anomalous dispersion.

1. Problem Statement

Photonic crystals have been studied for a number of years, primarily with applications in the optical regime. Photonic crystals can also play a beneficial role in the microwave band, particularly when wide bandwidth is a consideration. Photonic crystals offer the possibility of improving antenna directivity and efficiency with minimal losses. The purpose of this grant was to research and develop photonic crystal flat panel radiators for wideband high power antennas. These antennas are of great interest to the U.S. Army for use in communication systems, as well as in electromagnetic susceptibility studies. The research performed under the auspices of this grant studied these issues, as well as some fundamental questions regarding the nature of electromagnetic wave propagation and superluminal group velocities. The placement of an antenna on a defect state in a photonic crystal was found to enhance its radiation characteristics.

2. Summary of Recent Results

I. Integration of a Microstrip Patch Antenna with a Two-Dimensional Photonic Crystal Substrate

Introduction

Photonic crystals are a class of periodic metallic, dielectric, or composite structures that exhibit transmission (pass) and reflection (stop) bands in their frequency response [1,2]. These bands occur due to the constructive and destructive interference of the electromagnetic waves. For example, the stop band in a three-dimensional infinite crystal is referred to as a "forbidden" gap since the waves in *all* directions destructively interfere and are thus evanescent. The photonic crystals used in this work were fabricated by drilling holes in a dielectric host using standard machining techniques [1]. If the periodicity in a photonic crystal is perturbed (by either removing or adding a material with a different dielectric constant), creating a "defect," a state is created in the forbidden gap where an electromagnetic mode is allowed and localization of the energy occurs [1].

Photonic crystals are currently being introduced in many novel microwave applications. For example, they have been used as filters in microstrip lines [3], as high-power microwave components [4], and as substrates for printed antenna structures [5-8]. Theoretical descriptions of photonic crystals thus far have been limited to determining the dispersion curve in an infinitely periodic structure [9]. However, many of the applications listed above require the determination of the characteristics of a photonic crystal of finite size or with a finite ground plane. One effective approach to studying finite-sized crystals, as well as antenna applications of photonic crystals has been the finite-difference time-domain (FDTD) technique [10,11]. This technique was implemented in this work.

Microstrip patch antennas are, on the other hand, well understood and have found applications in communication systems, as well as many other systems that require compact antenna structures [12]. The conventional microstrip antenna is a metallic patch of arbitrary shape that is placed a certain distance, typically less than 0.01λ, above a metallic ground plane. They are typically excited using a coaxial probe from the ground plane as shown in the inset of Fig. 1, or by a microstrip line in the plane of the antenna [12]. Due to their resonant nature, however, microstrip patch antennas are inherently narrowband. Although many techniques have been presented to effectively increase the bandwidth of the patch antenna, many of the solutions are complicated or require multi-layer structures [12].

One of the simplest methods for increasing the bandwidth of a patch antenna is to increase the thickness of the dielectric substrate [12]. The increase in the dielectric thickness, however, results in the excitation of substrate and surface modes that remove energy from the main radiation lobe. If a photonic crystal is designed such that the frequency of the substrate mode overlaps the stop band frequencies, the excited substrate mode exponentially decays, reducing the energy lost into the substrate. In a crystal of infinite extent, the substrate mode would be evanescent and no energy would be lost. Yang et al. originally proposed that high-gain antenna structures could be obtained by printing an antenna on a *two-dimensional* photonic crystal [8]. In this section we

describe results where two-dimensional photonic crystals were employed as a means of eliminating the substrate and surface modes in a patch antenna. In addition, the two-dimensional photonic crystal antenna structure was fabricated with a defect in the periodicity at the patch antenna location, confining the energy under the antenna. It is anticipated that this energy confinement will yield a more efficient antenna structure.

Finite-difference-time-domain (FTDT) Studies

The finite-difference time-domain (FDTD) code used in this work was XFDTD® (Version 4.06), a commercial code available through Remcom, Inc. [13]. The code is based on the standard Yee cell geometry, and the values of the electric and magnetic fields are calculated in consecutive time steps [10]. The utility of the program is manifested in the ability to calculate S-parameters [10]. The Cartesian coordinate system was employed and the two antennas compared in this work are shown in Fig. 1 with the coaxial probe excitation shown in the inset. Two sets of simulations were performed. The initial sets of simulations were used to validate the code through experimental verification. The second sets of simulations were used to compare a conventional patch antenna with one that was integrated with a two-dimensional photonic crystal.

For the initial sets of simulations, the patch had a width of 8 mm in the x-direction and a length of 4.14 mm in the y-direction. The antenna geometry was broken up into a grid of Δx=0.4 mm, Δy=0.414 mm and Δz=0.25 mm in a space of 75x50x25 cells. The width of the antenna was 20Δx cells and the length of the antenna was 10Δy cells. The substrate in the FDTD calculation was 1.25 mm, thereby occupying 5 cells in the z-direction with a dielectric constant of 10.2. The antenna was excited 1.66 mm centered from the bottom edge of the antenna. The time step used was 0.6294 psec, which is set to the Courant limit for a general three-dimensional grid [14]. The ground plane was assumed to be infinite in extent; all other boundaries were set to be absorbing (Liao type).

For the second sets of simulations, the size of the FDTD space was increased such that the effects of the two-dimensional photonic crystal could be studied. The patch had a width of 8 mm in the x-direction and a length of 4 mm in the y-direction. The antenna geometry was broken up into a grid of Δx=0.1 mm, Δy=0.1 mm and Δz=0.4233 mm in a space of 120x135x35 cells. The substrate in the FDTD calculations was 1.27 mm thick, thereby occupying 3 cells in the z-direction and had a dielectric constant of 10.2. The time step was taken to be 1.211 psec, which was again set to the Courant limit for a general three-dimensional grid. For the modeling of the ground plane, two cases were considered in the simulation. The first case was where the substrate was placed directly on the lower boundary, where the boundary is a perfect electric conductor (PEC). The ground plane in this case was infinite in extent. The second case that was considered was where the substrate was suspended in the FDTD space 10 cells above an absorbing boundary and a finite PEC layer was used as a ground plane. In both cases all remaining boundary conditions were set to be absorbing. With the simulations mentioned above, the finite ground plane effects could be investigated.

The excitation source of the antenna was a Gaussian pulse with a width of 121 psec. The coaxial probe excitation of the antenna is shown on the inset of Fig. 1. It was found that a thin wire was the best type of excitation suited for obtaining reasonable agreement

with the experimental results. For the initial set of simulations, the code was run for 10,000 time steps that took approximately thirty minutes on a Pentium Pro, 300 MHz machine with 256 MB of RAM. For the second set of simulations, the code ran for approximately 5 hours on the same machine.

Experimental Results

Two antennas were built for measurement. Both had a width in the x-direction of 8 mm and a length in the y-direction of 4.14 mm and were fabricated on a RT-Duroid 6010 substrate with a dielectric constant of 10.2. The thickness of both substrates was 1.27 mm (50 mils). The first antenna had a uniform dielectric substrate as shown in Fig. 1(a), and the second antenna had the two-dimensional photonic crystal integrated, which was obtained by drilling holes into the substrate as shown in Fig. 1(b). The photonic crystal substrate was a triangular lattice with lattice constant of 1.38 cm and a hole diameter of 1.27 cm and was designed to have a gap at approximately 9 GHz [1]. This gap design was based on a photonic crystal that was infinite in extent in the transverse direction. The exact mode pattern of the grounded microstrip structure in a two-dimensional periodicity is currently under investigation.

An HP8340A sweep generator was used to excite the antenna structures and a Boonton 4200 power meter in conjunction with an X-band horn antenna was used to detect the radiation. The standard gain horn antenna was placed approximately 4.5 m away from the transmitter. The transmitting antenna was attached to a computer controlled rotary stage such that pattern measurements could be made. The excitation frequency for the antennas was determined by measuring the minimum return loss (S_{11}) using an HP8510 network analyzer.

The network analyzer measurements are compared to the FDTD calculation for the conventional patch antenna in Fig. 2, where the solid line is S_{11} measured using the network analyzer and the line with the markers is the calculated result using XFDTD®. The calculated results are based on the first set of simulations and are in excellent agreement with the experiment.

Figure 3 is the result of the second simulation where a finite ground plane was compared to the infinite ground plane for a conventional patch antenna. Recall that the second simulation has a coarser grid compared to the first simulation, such that the effects of a large ground plane and the photonic crystal could be investigated. The solid line is the infinite ground plane and the dashed line is the finite ground plane. Note that there is a slight increase in the resonance bandwidth of the finite crystal and a 4.5 dB increase in the depth of the resonance. However, there is no variation in the resonant frequency. In addition, the finite ground plane causes off-resonance ringing.

Figure 4 shows the measured pattern of the conventional patch antenna as a function of the size of the ground plane. Note that, as the size of the ground plane is increased, the effect is a variation in the back lobe level. The lobes in a microstrip antenna pattern are due to the finite size of the ground plane. Given an infinite ground plane, there would be no back lobes. Figure 4(a) is the result for a 5" square ground plane. Note that the scale on each antenna pattern measurement is 2 dB/division. For the 5" square ground plane the maximum back lobe is 9 dB below the main beam and occurs at approximately 310°. For the 6" square ground plane in Fig. 4(b), the maximum back

lobe is 11 dB below the main beam and is at 290°. For the 9" square ground plane in Fig. 4(c), the maximum back lobe is 10 dB below the main beam at 240°.

Figure 5 presents the measured antenna patterns for the patch antenna with the two-dimensional photonic crystal incorporated as shown in Fig. 1(b). For the 5" square ground plane in Fig. 5(a), the maximum back lobe is 13 dB below the main beam at approximately 285°. For the 6" square ground plane in Fig. 5(b), the maximum back lobe is 11 dB below the main beam at 265°. For the 9" square ground plane in Fig. 5(c), the maximum back lobe is 15 dB below the main beam at 250°. Therefore, the addition of the two-dimensional photonic crystal to the conventional patch antenna reduces the back lobe levels for the ground plane sizes considered here.

Figure 6(a) is the S_{11} measurement for the conventional patch antenna. The resonant frequency of the conventional antenna is not a function of the size of the ground plane. On the other hand, Fig. 6(b) is the S_{11} measurement for the two-dimensional photonic crystal antenna with the 6" ground plane. Note that the antenna resonance is broadened in comparison to the conventional antenna, however, the magnitude of the resonance is lower. The response of the conventional patch has a resonance of 14 dB at a resonance frequency of 9.324 GHz. The photonic crystal antenna has a resonance of 7.5 dB at a frequency of 9.044 GHz. The weak resonance is due to the poor match of the source to the antenna, which can be improved by adjusting the location of the feed.

Figure 7 presents results from the calculation of the conventional patch antenna based on the second set of simulations, shown as the solid line, and the conventional patch antenna integrated with a two-dimensional photonic crystal indicated by the dotted line. As in the experiment, the resonance of the photonic crystal antenna is weaker. However, the resonance frequency does not vary. This implies that the antennas that were experimentally measured were not identical. Therefore, a shift in the resonant frequency should not be expected when a photonic crystal antenna is used.

Summary

A two-dimensional photonic crystal was integrated with a conventional rectangular microstrip patch antenna. The properties of this structure and the effects of a finite sized ground plane on the resonance frequency were studied using an FDTD code. Calculations compare favorably with experiments. For a finite size ground plane, the resonance bandwidth is slightly larger and the resonance is deeper than the case of the infinite size ground plane. Antenna pattern measurements were used to assess the importance of the size of the ground plane. There is an increase in the back lobe level as the ground plane size is reduced. The back lobes are due to energy that propagates away from the antenna in the form of a surface wave and/or a substrate mode. Once the energy reaches the edge of the ground plane, edge currents re-radiate into the back of the antenna. Integration with the photonic crystal reduces the level of the edge currents.

The photonic crystal substrate was fabricated with a defect state under the antenna site. This defect state stores the energy under the antenna. The effects of this defect are currently under investigation. Preliminary results indicate that the radiated power is increased due to the energy storage under the antenna. Finally, conventional design tools for microstrip patch antennas are insufficient to determine the optimal coupling into the

antenna. This is shown in the measurements and calculations that compared the conventional patch antenna to the photonic crystal antenna. A design tool is currently being developed to optimize the incorporation of the antenna with the photonic crystal.

II. Frequency domain detection of superluminal group velocity in a One Dimensional Photonic Crystals (1DPC)

Introduction

Since the introduction of Maxwell's equations in 1865, and later experimental verification of propagating electromagnetic waves by H. Hertz [15] in 1888, the velocity by which these disturbances travel has received much attention. The first mention of group velocity actually predates Maxwell's equations and appeared in the published abstracts of Hamilton [16] dated 1839. The concept was reintroduced by Stokes in 1876 for hydrodynamics, and was generalized into the modern form by Rayleigh in 1877 [17]. In 1905, Einstein's work in special relativity established the speed of light in vacuum (c) as a universal limit. Almost contemporaneously, it was known that phase velocity and, more importantly, group velocity in regions of anomalous dispersion could exceed c. Sommerfeld in 1907 and Brillouin in 1914 investigated this apparent paradox and in their authoritative work [18] clearly showed that, for a step-modulated signal propagating through a Lorentz gas, the forerunners always travel with speed equal to c.

In a 1932 paper, MacColl [19] argued that a transmitted wave packet tunneling through a potential barrier would appear on the other side of the barrier almost instantaneously. Later, in a paper that reignited the most recent debates on superluminality and tunneling, Hartman [20] put MacColl's argument on more solid ground. His analysis implied that for thick enough barriers, the tunneling time is indeed superluminal. More recently, possibly because of technical difficulties in performing an experimental measurement of the tunneling time for electrons, attention has turned to the analogous problem of electromagnetic propagation (photon tunneling) via evanescent modes through photonic barriers. It is well understood that in its stationary form, the Schrödinger equation and the Maxwell-Helmholtz wave equation are mathematically identical [21]. In principle, an experiment involving electromagnetic propagation can shed light on the problem of electron tunneling [22-24].

In the optical regime, Chiao and coworkers [25] recently found the tunneling velocity for a single photon through a 1DPC to be superluminal. Spielman et al. [26] used femtosecond optical pulses to study tunneling through a 1DPC. They concluded that the tunneling time is indeed superluminal and were able to measure advances up to 6 femtoseconds.

Direct investigation of superluminal electromagnetic wave propagation are also possible using microwaves. One of the first experiments was conducted by Ranfagni et al. [27]. At first, their evanescent (or tunneling) region consisted of an undersized P-band waveguide connected at both ends to an oversized X-band waveguide. Complicated by the dispersion and dissipation in the waveguide and spurious effects due to the transition from X to P-band, their original results were inconclusive. In later efforts they were able to improve their signal-to-noise ratio and obtain better experimental data [28]. They were

also able to measure the delay time of leaky waves for a pair of transmitting and receiving horn antennas [29]. The receiver horn was shifted or tilted with respect to the launcher and delay times less than the time required by light to traverse the separation in vacuum were obtained.

Another series of microwave experiments were performed by a German group [30-34]. Expanding on the work of Ranfagni, et al., they studied propagation through an undersized waveguide both in the frequency and time-domains. Using the Line-Reflect-Match waveguide calibration technique, they were able to remove most of the systematic errors in the experiment. Nimtz and Enders [34] briefly considered transmission through a 1DPC inserted into a hollow metallic waveguide. This meant that superluminal barrier crossing was occurring through both 1DPC and the dispersive under-sized waveguide. Moreover, in this work, and in all of their frequency-domain analysis, they used the Fourier transform to extend the frequency-domain network analyzer results to the time-domain. This required an assumption regarding the form of the incident wave packet. In addition, they used only the response function amplitude to calculate the time-domain signal. This assumed a constant phase for the response function, strictly true only for an infinitely long, cutoff waveguide or 1DPC.

In this study we present our results of wave propagation through a 1DPC using the concept of group delay, $\tau_g = -\partial\varphi/\partial\omega$, where φ is the phase of the response function. Within the stationary phase approximation, the group delay is a more natural approach to understanding propagation through finite length dispersive structures. To accurately measure phase, a powerful calibration technique was developed to eliminate systematic errors. These experiments were conducted in free-space, removing the aforementioned combined response effects and allowing close comparison with theoretical models.

Transfer Matrix Technique

Figure 8 depicts a 1DPC (optical multilayer) consisting of alternating layers of the dielectric Eccostock® and air. The structure exhibits frequency regions for which transmission is prohibited (band-gaps) and frequency intervals for which transmission is allowed (pass-bands). It is for signals propagating through the band-gaps of photonic crystals (PCs) that superluminal group velocities are expected.

In order to calculate the transmission properties of the finite 1DPC, standard transfer matrix techniques are followed [35]. The one period matrix **M** is given by

$$\mathbf{M} = \frac{1}{1-\rho_{i,j}^2}\begin{bmatrix} a & b \\ b^* & a^* \end{bmatrix}, \tag{1}$$

where

$$a = \exp\left[-i\left(\beta_i + \beta_j\right)\right] - \rho_{i,j}^2 \exp\left[i\left(\beta_j - \beta_i\right)\right], \tag{2}$$

$$b = -\rho_{i,j} \exp\left[i\left(\beta_i - \beta_j\right)\right] + \rho_{i,j} \exp\left[i\left(\beta_j + \beta_i\right)\right], \tag{3}$$

and with

$$\beta_k = \frac{2\pi}{\lambda_0} n_k d_k \cos(\theta_k), \quad k = i \text{ or } j. \tag{4}$$

Here λ_0 is the free-space wavelength, θ_i is the incident angle measured from the normal to the interface, $\rho_{i,j}$ is the TE or TM Fresnel reflection coefficient, n_k is the index of refraction and d_k is the thickness of the i or j region. Although conservation of energy requires **M** to be unimodular [det(**M**)=1], **M** is not unitary [36].

To calculate the transmission coefficient for a 1DPC consisting of N dielectric slabs, **M** must be raised to the Nth power. While it is possible to write the resultant matrix in terms of Chebyshev polynomials [37,38], here the final result is expressed in terms of the eigenvalues and eigenvectors of the one period matrix as [39],

$$\mathbf{M}^N = \mathbf{S}\,\Lambda^N\,\mathbf{S}^{-1}, \tag{5}$$

where Λ is a diagonal matrix of eigenvalues and **S** is the matrix of eigenvectors of **M**. In writing Eq. (5) it is only required that **M** have a complete set of eigenvectors (although the eigenvalues can be degenerate). Computationally, Eq. (5) reduces the problem of raising a matrix to the Nth power to raising a scalar to the same power. More importantly, since the eigenvalues and eigenvectors of **M** are known, a closed form expression for $\mathbf{M}^N$, and accordingly the transmission and reflection coefficients, can be obtained as given below:

$$t = \frac{(\lambda_1 - \lambda_2) e^{i\beta_k} \left(1 - \rho_{i,j}^2\right)^N}{\lambda_2^N (a - \lambda_2) - \lambda_1^N (a - \lambda_1)} = |t| e^{i\varphi}, \tag{6}$$

$$r = \frac{\left(\lambda_1^N - \lambda_2^N\right) b}{\lambda_1^N (\lambda_1 - a) - \lambda_2^N (\lambda_2 - a)} = |r| e^{i\phi}, \tag{7}$$

where λ_1 and λ_2 are the eigenvalues of **M**, expressed as

$$\lambda_{1,2} = \left(1 - \rho_{i,j}^2\right)^{-1} \times \left[\cos(\beta_j + \beta_i) - \rho_{i,j}^2 \cos(\beta_j - \beta_i) \pm \sqrt{\left[\cos(\beta_j + \beta_i) - \rho_{i,j}^2 \cos(\beta_j - \beta_i)\right]^2 - \left(1 - \rho_{i,j}^2\right)^2}\,\right], \tag{8}$$

with the plus sign for λ_1 and the minus sign for λ_2. Equations (6) and (7) are unchanged if n_i or n_j are complex.

Having acquired complex transmission and reflection coefficients, the transmission and reflection group delays now can be calculated as

$$\tau_g^t = \tau_g = -\frac{\partial \varphi}{\partial \omega} = -\frac{\partial\, Arg(t)}{\partial\, \omega} \tag{9}$$

$$\tau_g^r = -\frac{\partial \phi}{\partial \omega} = -\frac{\partial\, Arg(r)}{\partial\, \omega} \quad . \tag{10}$$

Consequently, the normalized group velocity of the transmitted wave is given by

$$\frac{v_g}{c} = \frac{L_{pc}}{c\tau_g} \quad , \tag{11}$$

where L_{pc} is the total physical length of the finite 1DPC,

$$L_{pc} = (N-1)(d_i + d_j) + d_j \, . \tag{12}$$

Experimental Results

Figure 9 shows the free-space experimental set-up. It consists of two standard K-band horn antennas (SHA's) connected to ports 1 and 2 of an 8722D HP Network Analyzer (NA), configured to measure the transmission coefficient (t or S_{21}). The set-up is enclosed in an anechoic chamber to reduce stray signals. In order to minimize edge diffraction, Eccostock® slabs with large transverse dimension (31 cm × 31 cm) along with a pair of microwave collimating and focusing lenses were used. In addition to diffraction, there are at least two other sources of error: the effect of the experimental components such as the SHAs and lenses on the measurement, and the loss in the detected signal due to the transmitter-receiver misalignment and propagation losses.

With recent advances in non-coaxial calibration procedures for the NA [40,41] such as the "Thru-Line-Reflect" (TRL) calibration technique, it is possible to systematically remove the components' influences on the measured value of S_{21}. In this case the "Thru" standard is a free-space transmission line of length 58.9 cm, while the "Line" standard is a free-space transmission line of length 59.24 cm [41]. The "Reflect" is a copper plate set mid-way between transmitter and receiver. The "Thru" is used to set the reference plane from which the transmission loss ($|t|$) and insertion phase (φ) are measured. Performing the TRL calibration in free-space eliminates any contributions from waveguide dispersion and losses associated with inserting the 1DPC into a waveguide [34]. This experimental design simplifies extracting the response of the 1DPC from its surroundings.

After calibrating the system (without the 1DPC), a reference plane of unit magnitude for $|t|$ and zero phase for φ is established mid-way between the two SHA's. At this point, the 1DPC is inserted and the receiver horn is moved back exactly by distance L_{pc}. This ensures that the measured transmission coefficient is solely due to the 1DPC. Clearly, moving the transmitter backward introduces some propagation losses. This small loss (t^{prop}) can be measured and its contribution can be deconvolved from the measured response according to

$$t^{measured}(\omega) = t^{PC}(\omega)\, t^{prop}(\omega) \, , \tag{13}$$

where t^{PC} is the desired response function. To precisely control the backward movement of the receiver antenna, the insertion phase introduced by traveling the distance L_{pc} can be monitored. By averaging traces, phase variations as small as one degree can easily be detected. From Eq. (14) below, it is clear that at 21.5 GHz, a phase error of one degree corresponds to accuracy of 0.004 cm in length.

$$\Delta z = \frac{\Delta \varphi \, c}{2 \pi \nu}. \tag{14}$$

Figure 10 shows the calculated transmission coefficient magnitude and phase [$|t^{pc}(\omega)|$, φ], and the raw measured values for a 1DPC with N=3. Despite the fact that the signal amplitude has decreased by a factor of 20 in the band-gap, experiment and theory agree quite well. The average complex index of refraction for Eccostock® was measured to be 3.4 - i 0.002 over the frequency range of the interest. The thicknesses of the Eccostock® slab and the air-spacer were determined to be 1.33 and 1.76 cm, respectively. The high value of the index for Eccostock® provides the opportunity to use a minimal number of slabs to obtain the desired response, further minimizing the effect of propagation losses. On the other hand, compared to other microwave materials such as polycarbonate, Plexiglass or Teflon, Eccostock® demonstrates more inhomogeneities. This inhomogeneity can account for the small differences between the theoretical and experimental results. An interesting aspect of the set-up shown in Fig. 9 is that the same arrangement and calibration technique can be used to measure the real and imaginary part of the index of refraction for any sheet materials. Simply by measuring $|t|$ and φ for one slab, and with the help of the Eq. (6) with N=1, the real and imaginary part of the index can be calculated over the frequency range of interest [42].

Finally, upon closer examination of measured transmission coefficient, some small ripples in the response of the 1DPC is detectable. Within the theory of operation for the NA, these small modulations are well understood and are attributed to an imperfect source and load mismatches [43]. Unfortunately, these effects cannot be removed by using the TRL calibration technique. More importantly, according to Eqs. (9) and (11), the phase of the transmission coefficient is of greatest interest. Figure 11 is the calculated and measured unwrapped phase for a 1DPC with three, two and one dielectric slabs. As might be suspected, with increasing N, the finite length 1DPC approximates the infinite 1DPC more closely, and in the limit of $N \to \infty$, the phase of the transmitted wave must approach a constant value [44]. This behavior is clearly exhibited in Fig. 11.

To obtain the group delay or group velocity, the curves depicted in Fig. 11 must be differentiated. The application of the differential operation on a data containing noise amplifies the noise and may lead to spurious effects. On the other hand, smoothing the phase data prior to differentiation is an arbitrary process that gives results which vary critically with the smoothing parameters. The approach used here is to obtain the best nonlinear least square fit to the experimental data. Since, the comparison between the theory and measurement (Fig. 11) is good and the theoretical model (Eq. 6) for the insertion phase of 1DPC is well established, the best fit to the phase data can be obtained as a function of the dielectric and spacer thicknesses (d_j, d_i) and dielectric index of refraction (n_j). A Fortran program based on the IMSL subroutine DBCLSF, which uses a modified Levenberg-Marquardt algorithm and a finite-difference Jacobian to obtain the

best least square fit was developed. Figure 12 shows the result of the least square fit to the phase data of Fig. 11 together with applying Eqs. 9 and 11 to determine the normalized group velocity of a 1DPC with one, two and three dielectric slabs.

Along with the velocities derived from the fit (dotted curves), the nominal group velocities calculated from measured values of thicknesses and the indices [45] are also shown (solid curves). The fitting parameters for the case N=3 were $d_i = 1.794$ cm, $d_j = 1.399$ cm, and the real part of the Eccostock® index (n_j') was 3.216 [46].

A closer examination of Fig. 12 reveals that, while one dielectric slab (N=1) is insufficient to produce superluminal group velocities, two slabs are sufficient to set up the interferences resulting in a group velocity exceeding c. In the next section, the sensitivity of the normalized group velocity to the experimental parameters will be discussed.

Sensitivity Analysis

As the peak group velocity depicted in Fig.12 occurs in the region of maximum attenuation of the transmitted signal, it is important to analyze the experimental uncertainties involved. In general, the measured phase is a function of five variables: frequency (ν), spacer index (n_i), spacer thickness (d_i), dielectric slab index (n_j), and thickness (d_j).

The HP Network-Analyzer 8722D has a 1 Hz frequency resolution and an accuracy of ±10 ppm [40]. In the above experiment, the frequency interval between two adjacent points was set to 10 MHz, and the "step sweep" mode of the analyzer was used in order to obtain greater frequency accuracy. In addition, since the spacer is nominally air, the spacer index (n_i) is taken as unity. However, the remaining three variables deserve a closer look.

In general, the variation of any function in terms of a given variable can be approximated by a difference equation. For example, variation of the normalized group velocity with respect to spacer thickness is given by

$$\Delta\left(V_g / c\right) \approx \Delta d_i \frac{\partial\left(V_g / c\right)}{\partial d_i} = \Delta d_i \frac{2\pi}{c\left(\partial\varphi/\partial\upsilon\right)^2}\left[\left(1-N\right)\frac{\partial\varphi}{\partial\upsilon} + L_{pc}\frac{\partial}{\partial d_i}\frac{\partial\varphi}{\partial\upsilon}\right], \qquad (15)$$

where $\partial\varphi/\partial\upsilon$ is proportional to group delay. Expressions for the variation of normalized group velocity with respect to the other variables (d_j, n_j) are similar to Eq. (15). In calculating the derivatives, it is assumed that the phase is a function of frequency and one other independent variable (e.g., d_i), while the other two variables (e.g. n_j,d_j) are assumed to be constant. A Fortran program using the IMSL routine DBS2DR was written to compute the two-dimensional tensor-product spline interpolant and its derivative. The results for given nominal values [45] of the variables for the case N = 3 are depicted in Fig. 13.

From Fig. 13 it is evident that the experimental measurement is insensitive to uncertainty in parameters at mid-gap or equivalently, at the peak group velocity. In general, the experimental group velocity is most sensitive to the dielectric slab's thickness with a maximum absolute value of 42.2 over the range of 20 to 23 GHz. On the other hand, using the phase measurement technique described by Eq. (14) or by using other methods, accuracies up to 0.004 cm are easily attainable. This means that

maximum absolute error in normalized group velocity due to the dielectric-slab thickness is about 0.17. The maximum error over the range for which superluminal behavior is exhibited (approximately 21 to 22 GHz) is 0.14. The experimental errors due to spacer thickness over the entire frequency range of 20 to 23 GHz is even smaller, since the maximum absolute value of $\frac{\partial\left(V_g / c\right)}{\partial d_i}$ is 6.57 as compared to 42.2.

Finally, analysis of the experimental errors associated with the measured Eccostock® index of refraction were based on measurement of the dielectric constant of 1.33 cm of air after the TRL calibration had been performed. These result in a maximum uncertainty in the Eccostock® index of approximately 0.01. Given the maximum absolute value for $\partial\left(v_g / c\right)/\partial n_j$ over the frequency range 20 to 21 GHz of 14.2, experimental errors in normalized group velocity of the order of 0.14 can be expected. Again, this error decreases to zero at mid-gap. From the above analysis it is clear that experimental errors are incapable of placing the normalized group velocity depicted in Fig. 12 below the light line.

A few remarks regarding the zeroes of the derivatives shown in Fig. 13 are in order. These represent frequencies at which the sensitivity of the measured variable (group velocity) with respect to the experimental parameters is identically zero. From a physical point of view, the insensitivity at the mid-gap occurs since the 1DPC exhibits minimal group velocity dispersion at frequencies around 21.7 GHz. This minimizes the term in the brackets of Eq. 15. The zero crossings at the band-edges occur because the group delay ($-\partial\varphi/2\pi\partial\nu$), is very large and the term outside the brackets in Eq. 15 dominates. From a technological point of view, the ability to design optical multilayers or delay lines for which the desired response is insensitive to variations in material parameters is of great importance. In fact, the inverse of the problem presented in this manuscript can be addressed by solving expressions such as Eq. (15) for the dielectric-slab and spacer thicknesses and indices, in order to design dielectric mirrors or delay lines that are less sensitive to component variations.

Summary

This section of the final progress report described the detection of superluminal group velocities in the frequency domain. Diagonalization of the transfer matrix is used to obtain analytical closed form expressions for both transmission and reflection coefficients. Measuring a 1DPC in free space enables removal of extraneous dispersion and dissipation and allows de-embedding the 1DPC properties. An experimental protocol based on the TRL calibration procedure was described resulting in good agreement between the experimentally measured and theoretically calculated phases. Accurate measurement of the transmission phase allows calculation of the group delay and group velocity.

The ability to actually measure superluminal group velocities questions the traditional notion that in regions of resonances, group velocity is "...not a useful concept

..." [47] or has "...no longer any appreciable physical significance..." [48]. However, it must be emphasized that this superluminal behavior is in no way in contradiction with special relativity or causality. In fact, it can be shown that superluminal group velocities are the consequence of linear time invariant systems which obey Kramers-Kronig relations and hence are inherently causal [49-53]. In the case of propagation through a 1DPC, the energy velocity remains subluminal [54], although, this is not a universal requirement for the energy velocity [52,53]. More importantly, under no circumstances does the front (forerunner) velocity exceed the speed of light in vacuum.

Figure Captions

FIG. 1: (a) Conventional patch antenna with a coaxial probe exciation (inset); (b) Two-dimensional photonic crystal that is integrated into the convenional patch.

FIG. 2: S_{11} measured (solid line) using a network analyzer and calculated (line with markers) using the FDTD code. There is excellent agreement between the calculations and the measurements.

FIG. 3: S_{11} calculated using the FDTD code. The effects of a finite ground plane are investigated. The solid line is an infinite ground plane and the dashed line is a finite ground plane. Note that the bandwidth of the resonance for the patch is slightly increased (the depth is slightly increased for a finite-sized ground plane).

FIG. 4: Measured antenna pattern for various-sized ground planes: (a) 5" ground plane; (b) 6" ground plane; (c) 9" ground plane. Note that the back lobe level decreases as the size of the ground plane increases.

FIG. 5: Measured antenna pattern for a two-dimensional photonic crystal integrated with a conventional patch antenna with a varying-sized ground plane: (a) 5" ground plane; (b) 6" ground plane; (c) 9" ground plane. Note that the back lobe levels are reduced when compared with a conventional patch antenna.

FIG. 6: (a) Measured S_{11} for a conventional microstrip patch antenna. (b) Measured S_{11} for an antenna integrated with a two-dimensional photonic crystal. Note that the depth of the resonance is reduced, implying a non-optimal excitation location.

FIG. 7: S_{11} calculated for the conventional patch antenna (dashed line) compared to the two-dimensional photonic crystal antenna (solid line). Note that the resonance is decreased due to a non-optimal excitation location.

FIG. 8: Schematic of the one dimensional photonic crystal (1DPC).

FIG. 9: Free-space experimental set-up.

FIG. 10: Measured (thin-dotted line) and calculated (thin-solid line) transmission phase and measured (thick-dashed line) and calculated (thick-solid line) transmission amplitude for a 1DPC with N=3.

FIG. 11: Calculated (solid line) and measured (dotted line) unwrapped transmission phase.

FIG. 12: Nominal (solid line) and fitted (dotted line) normalized group velocity for a 1DPC with N=3, 2, and 1.

FIG. 13: Sensitivity of the normalized group velocity to experimental parameters such as spacer thickness (solid line), dielectric-slab thickness (dashed line), and dielectric index of refraction (dotted line).

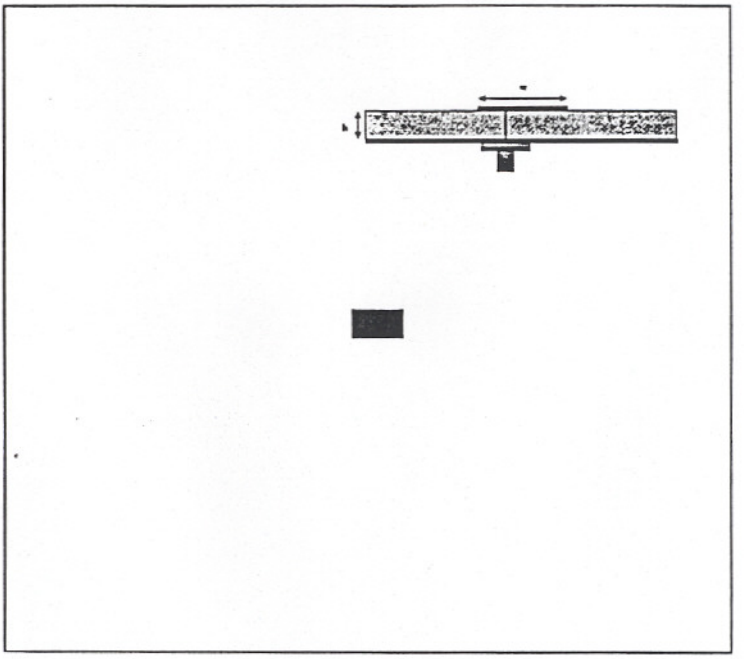

Figure 1(a)

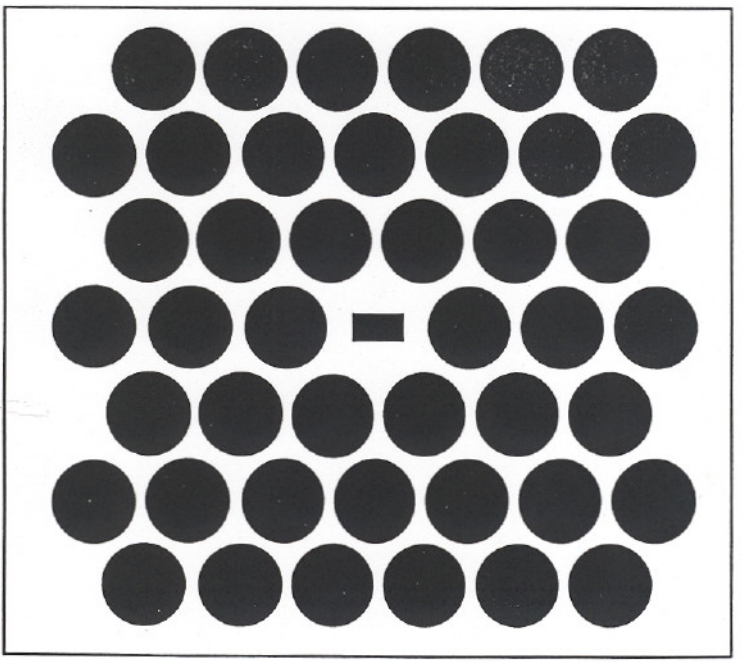

Figure 1(b)

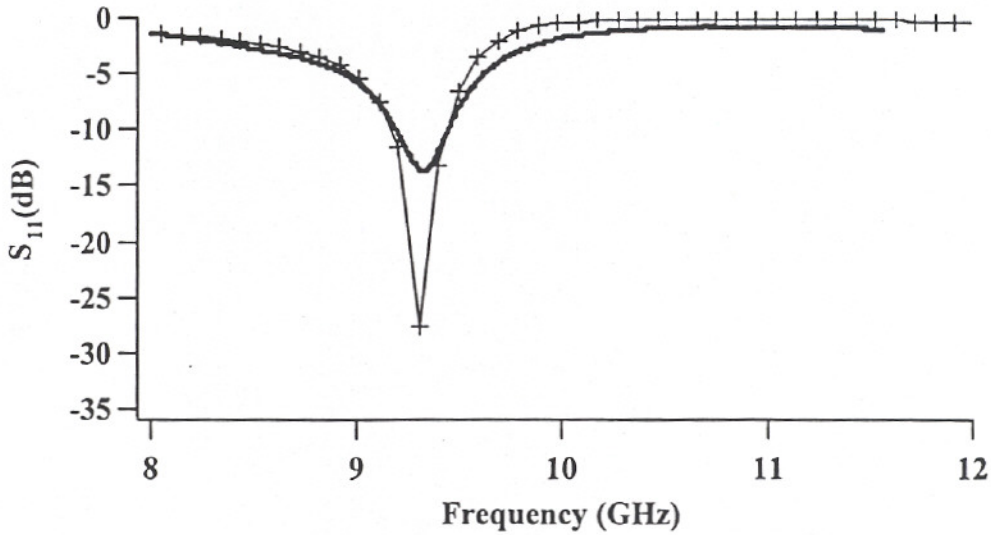

Figure 2.

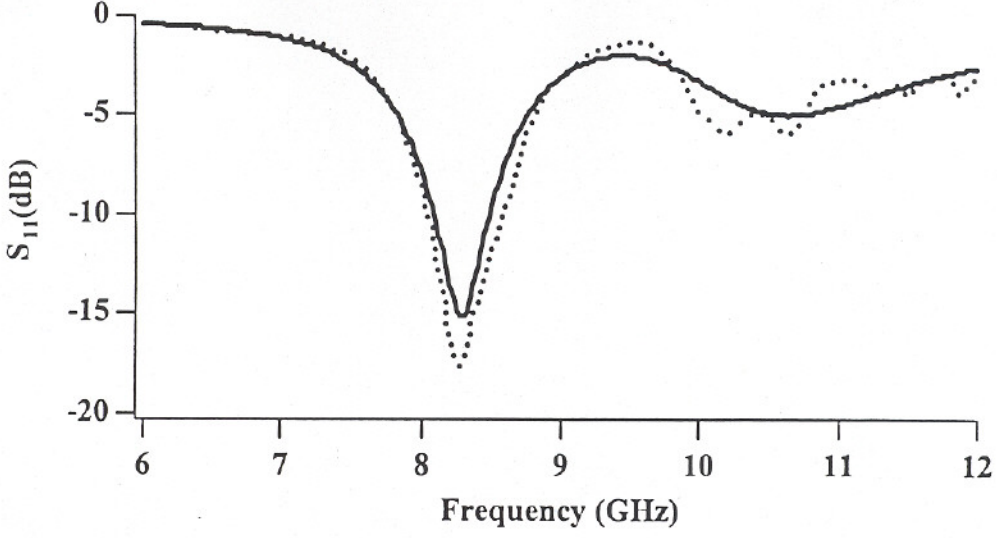

Figure 3.

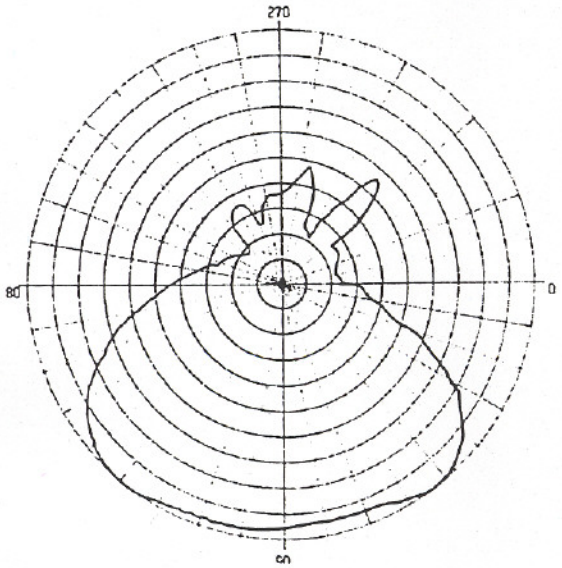

Figure 4(a)

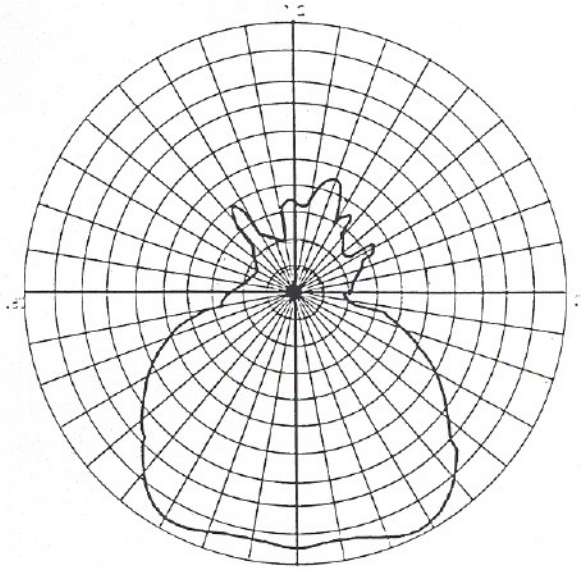

Figure 4(b)

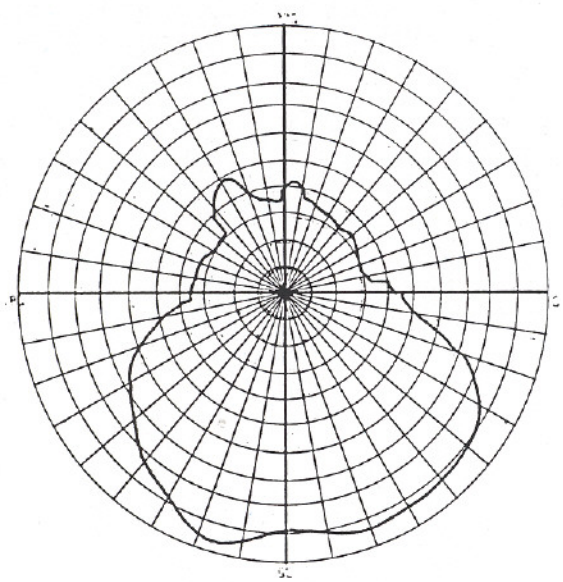

Figure 4(c)

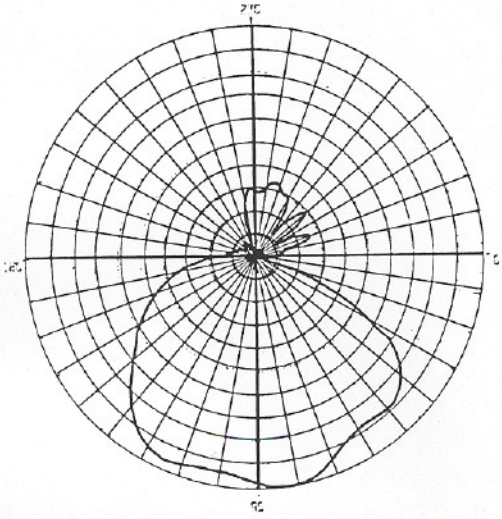

Figure 5(a)

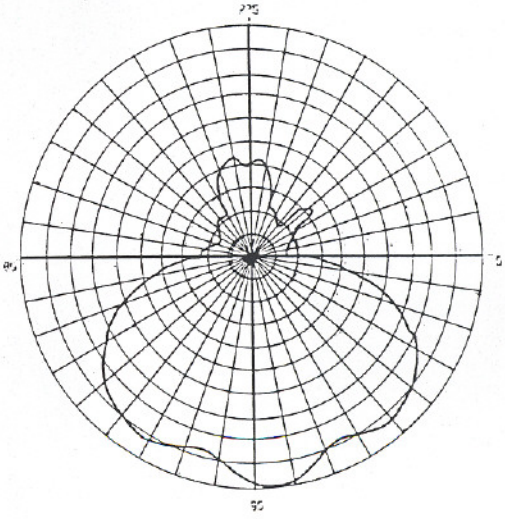

Figure 5(b)

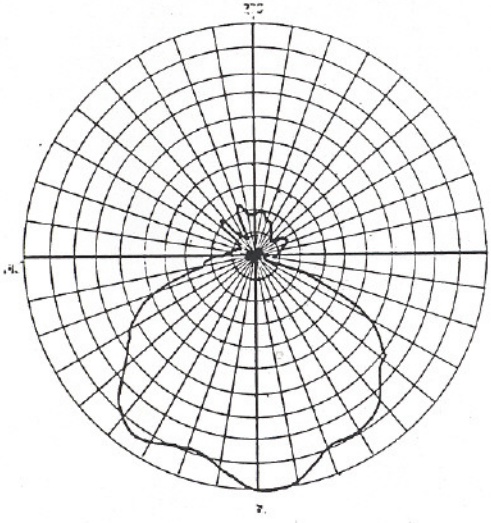

Figure 5(c)

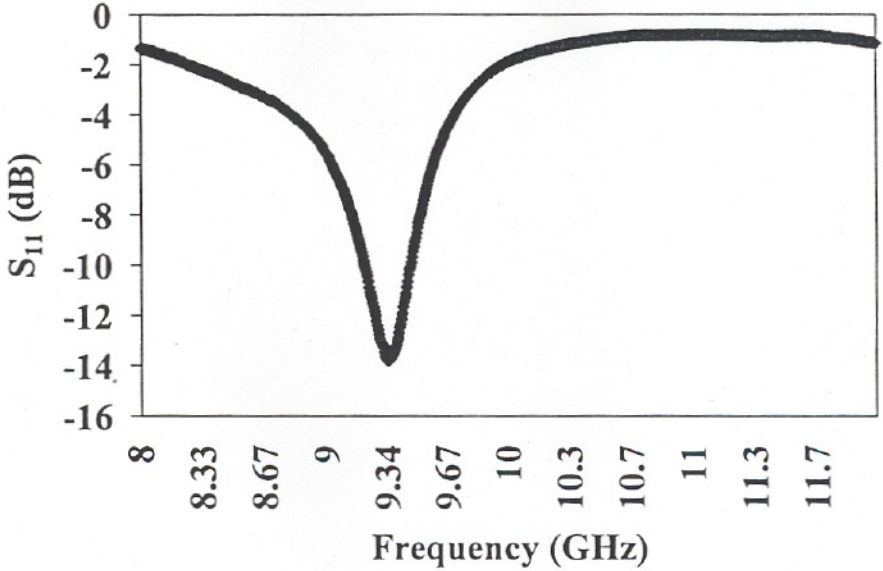

Figure 6(a)

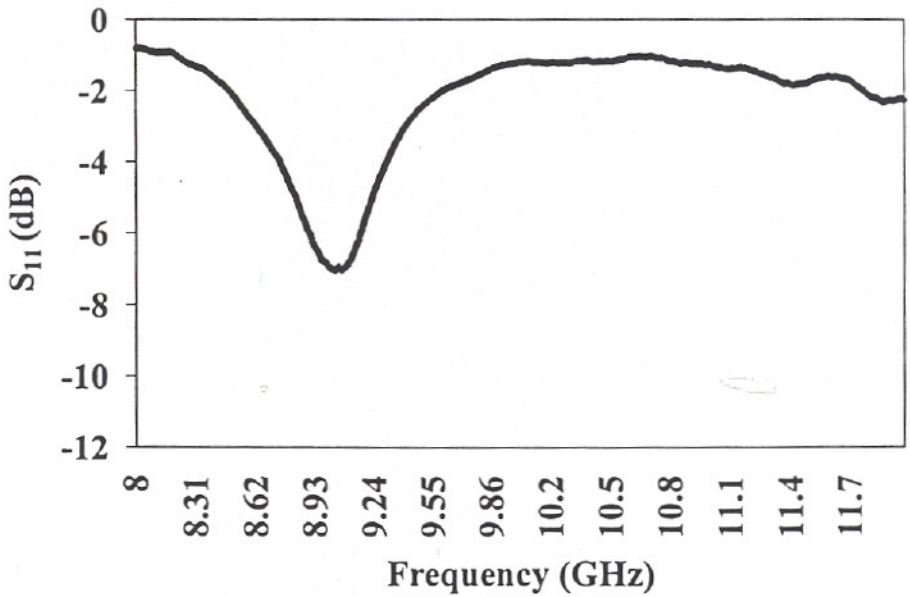

Figure 6(b)

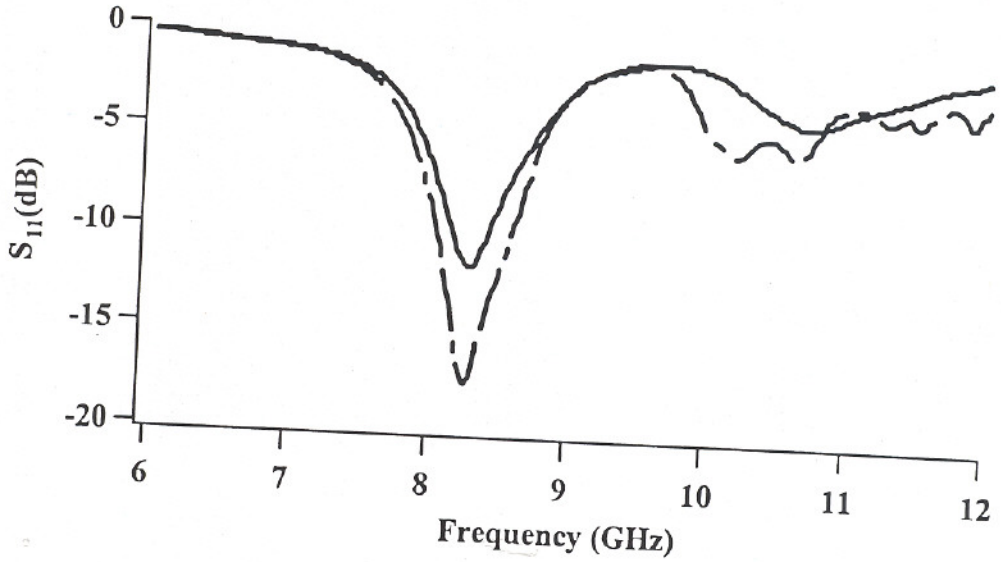

Figure 7.

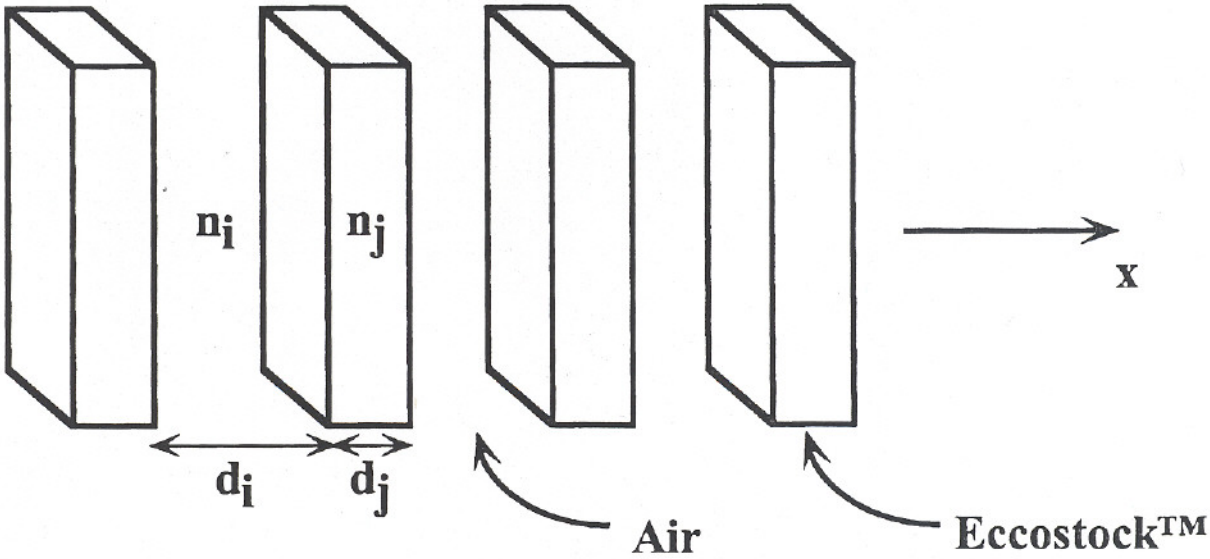

Figure 8.

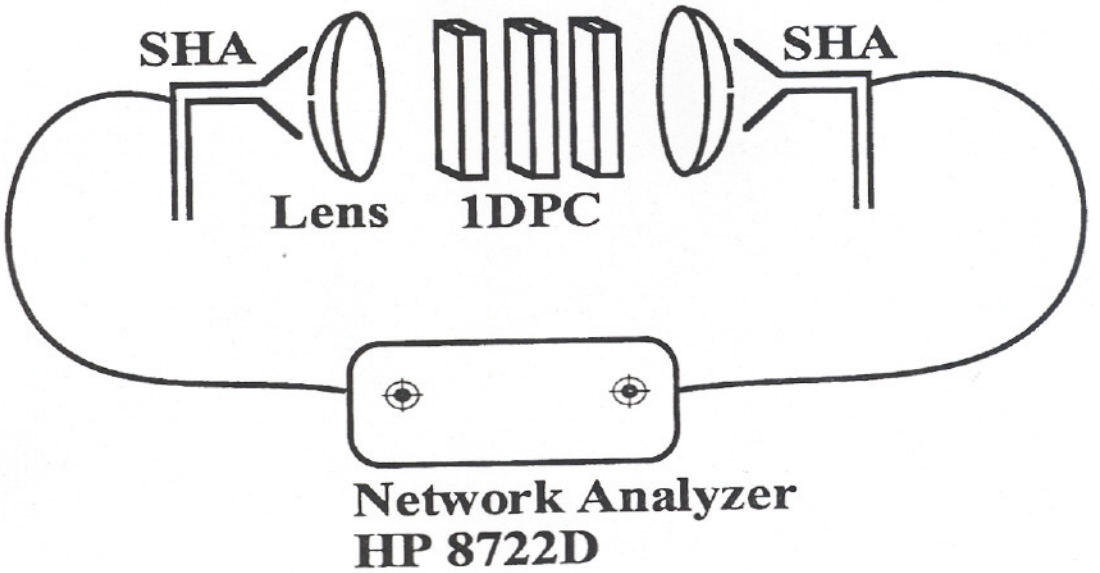

Figure 9.

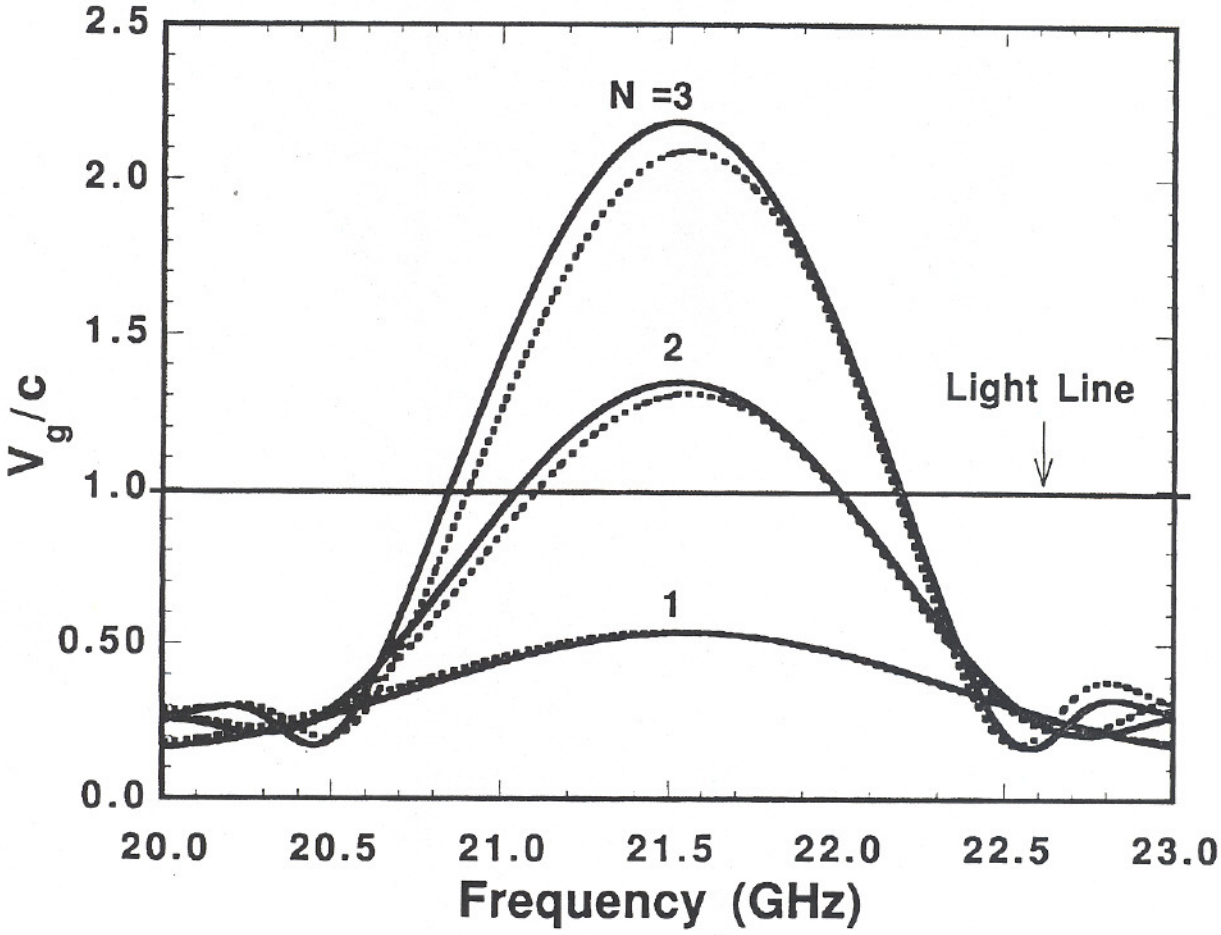
2.5
2.0
1.5
1.0
0.50
0.0
V_g/c
N =3
2
1
Light Line
20.0
20.5
21.0
21.5
22.0
22.5
23.0
Frequency (GHz)

Figure 10.

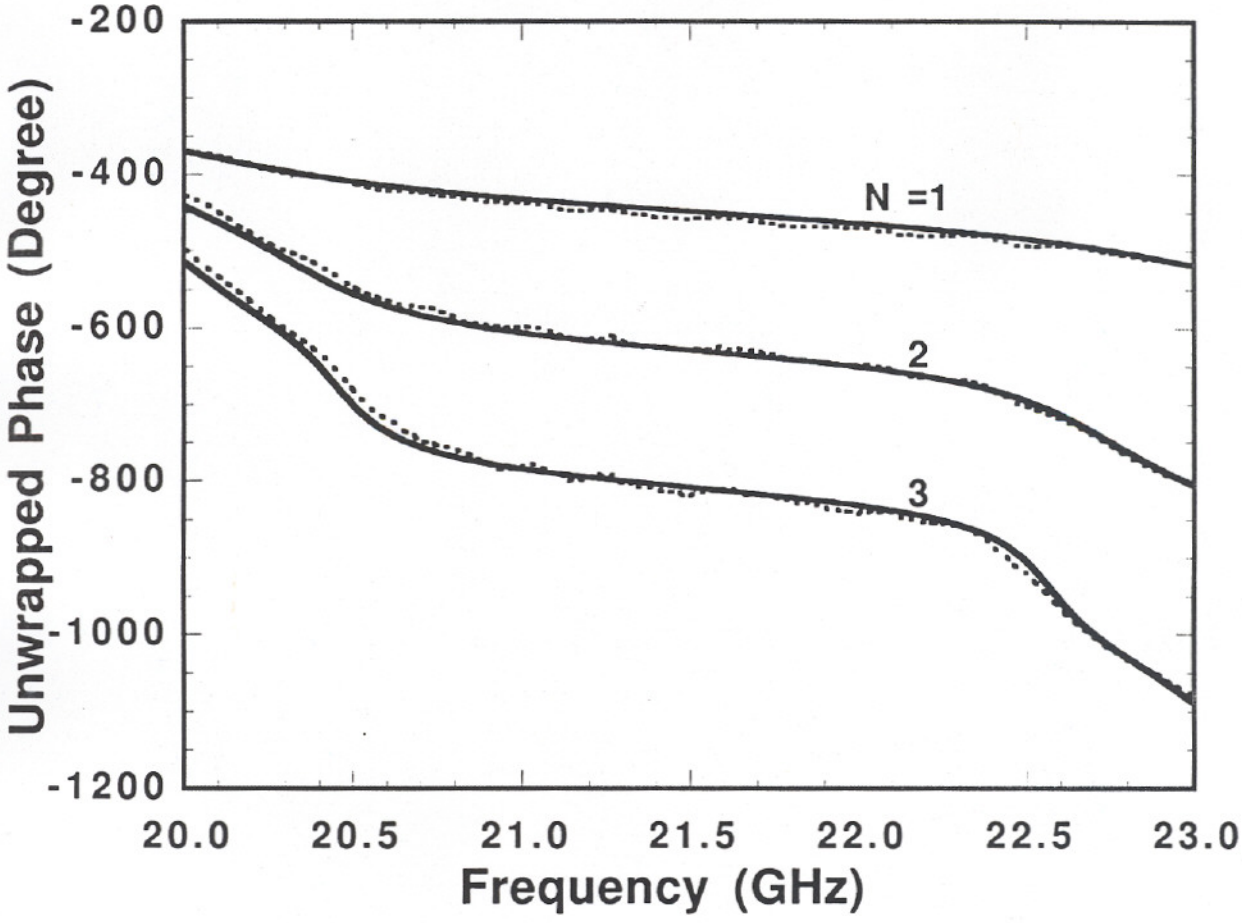
-200
-400
-600
-800
-1000
-1200
Unwrapped Phase (Degree)
N =1
2
3
20.0
20.5
21.0
21.5
22.0
22.5
23.0
Frequency (GHz)

Figure 11.

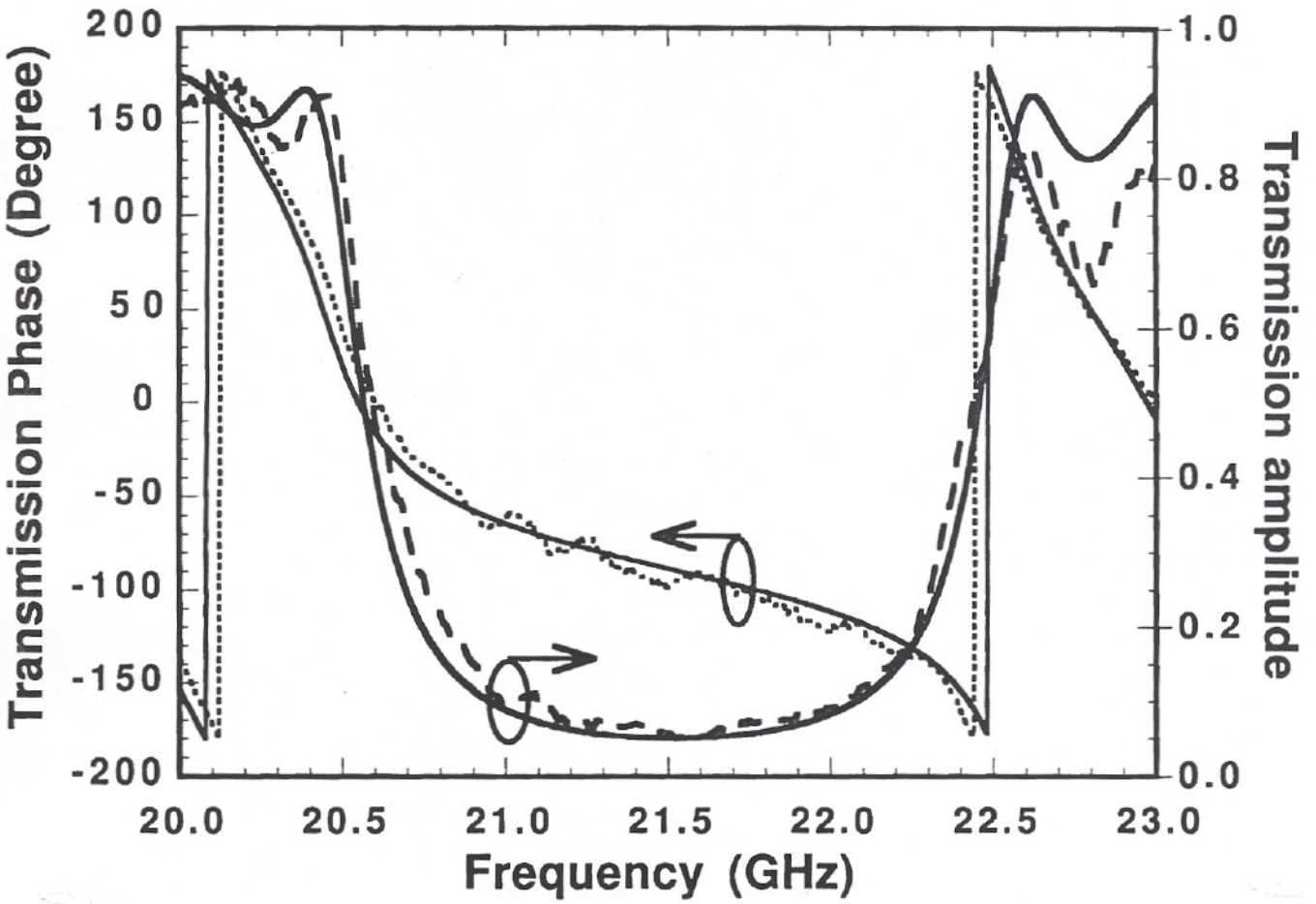
Transmission Phase (Degree)
200
150
100
50
0
-50
-100
-150
-200
Transmission amplitude
1.0
0.8
0.6
0.4
0.2
0.0
20.0
20.5
21.0
21.5
22.0
22.5
23.0
Frequency (GHz)

Figure 12.

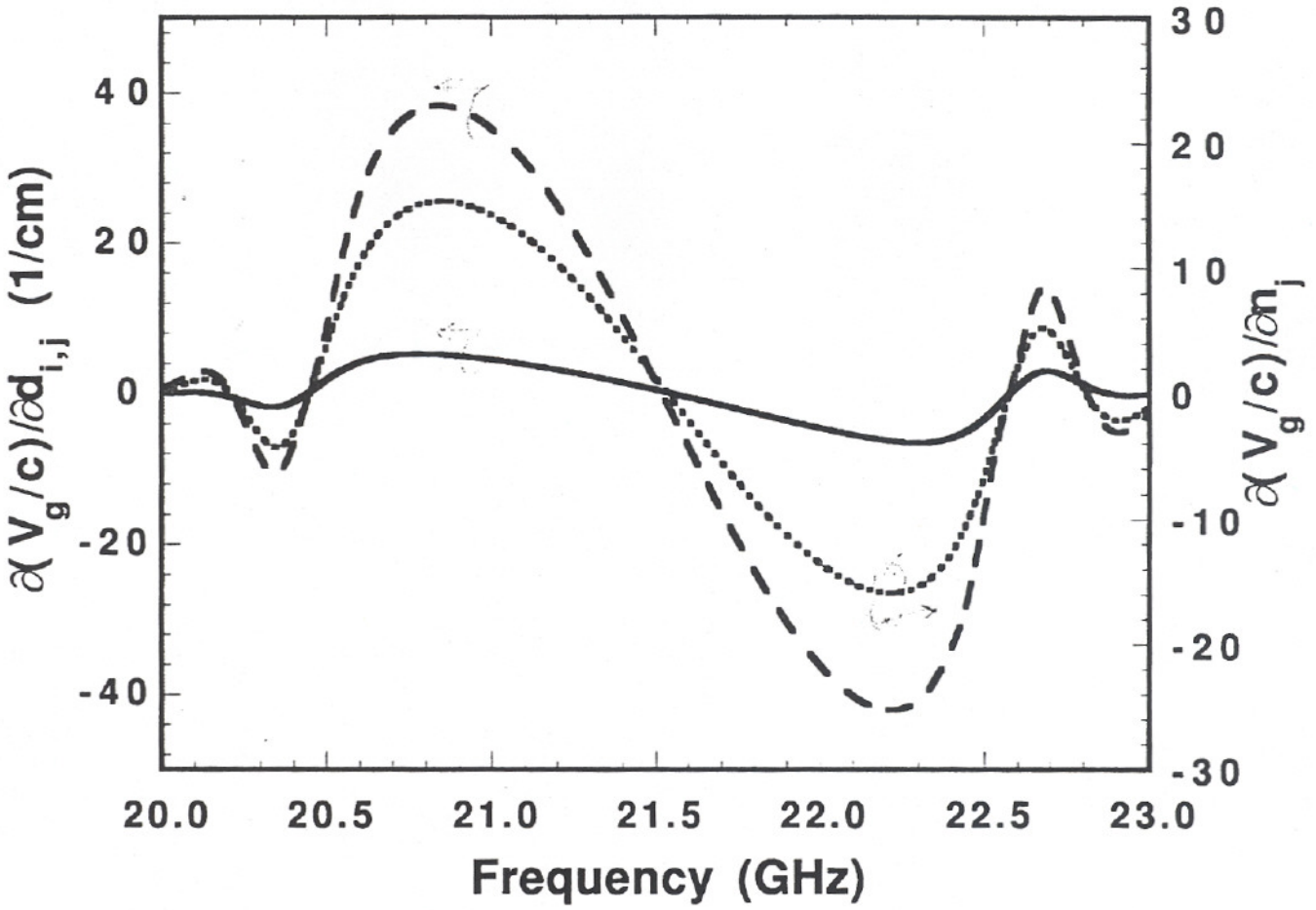
40
20
0
-20
-40
30
20
10
0
-10
-20
-30
20.0
20.5
21.0
21.5
22.0
22.5
23.0
Frequency (GHz)
∂(V_g /c)/∂d_i,j (1/cm)
∂(V_g /c)/∂n_j

Figure 13.

3. List of Presentations and Publications

1. K. Agi, "Properties and Applications of Microwave Photonic Crystals (Invited)," presented to New Jersey Section of the IEEE, Newark, NJ, Jan. 1998.
2. K. Agi, "Properties and Applications of Microwave Photonic Crystals (Invited)," presented to Aerospace Technology Group, Allied Signal, Inc., Morristown, NJ, Jan. 1998.
3. K. Agi, "Evolution of the Dispersive Properties of Photonic Crystals (Invited)," Physics Department Colloquium, University of Alabama, Huntsville, AL, Jan. 1998.
4. K. Agi, "Temporal Evolution of Dispersive Properties of Photonic Crystals (Invited)," presented to U.S. Army Aviation and Missile Command, Weapons Science Directorate, Red Stone Arsenal, AL, Jan. 1998.
5. K. Agi, K.J. Malloy, E. Schamiloglu, and M. Mojahedi, "Compact Microstrip Patch Antennas on Photonic Crystal Substrates (Invited)," USNC/URSI National Radio Science Meeting, Atlanta, GA, June 1998.
6. K. Agi, K.J. Malloy, E. Schamiloglu, M. Mojahedi, and E. Niver, "Integration of a Microstrip Patch Antenna with a Two-Dimensional Photonic Crystal Substrate (Invited)," to appear in Electromagnetics, Jan. 1999.
7. K. Agi, M. Mojahedi, B. Minhas, and K.J. Malloy, "Integration of a Microstrip Patch Antenna with a Two-Dimensional Photonic Crystal Substrate (Invited)," presented at Workshop on Electromagnetic Crystals (WECS), Laguna Beach, CA, Jan. 1999.
8. M. Mojahedi, E. Schamiloglu, K. Agi, and K.J. Malloy, "Frequency Domain Detection of Superluminal Group Velocity in One-Dimensional Photonic Crystals," submitted to Phys. Rev. E. Jan. 1999.
9. M. Mojahedi, E. Schamiloglu, F. Hegeler, G.T. Park, K. Agi, and K.J. Malloy, "Time-Domain Detection of Superluminal Group Velocity using Single Microwave Pulses," to be submitted to Phys. Rev. Lett., 1999.
10. M. Mojahedi, E. Schamiloglu, K. Agi, and K.J. Malloy, "A Simple Free Space Method to Measure Dielectric Constants and Superluminal Group Velocities," submitted to IEEE Trans. Microwave Theory and Tech., 1999.

4. List of Participating Personnel

1. Edl Schamiloglu, Associate Professor EECE, Co-PI.
2. Kevin Malloy, Associate Professor EECE, Co-PI
3. Kamil Agi, Research Engineer
4. Mohammad Mojahedi, Ph.D. Candidate (to be completed May 1999).

5. Report of Invention

1. K. Agi and K.J. Malloy, "Microstrip Patch Antennas on Two-Dimensional Photonic Crystals Incorporating Defects in the Periodicity," Invention disclosure filed with the University of New Mexico Patent Office, Docket Number UNM-518, December 15, 1998.

6. References

[1] J.D. Joannopoulos, R.D. Meade and J. N. Winn, *Photonic Crystals: Molding the Flow of Light* (Princeton University Press, New Jersey, 1995).

[2] E.R. Brown and O.B. McMahon, "Large Electromagnetic Stop Bands in Metallo-dielectric Photonic Crystals," *Appl. Phys. Lett.*, Vol. 67, no. 15, Oct. 1995.

[3] V. Radisic, Y. Qian, R. Coccioli and T. Itoh, "Novel 2-D Photonic Bandgap Structure for Microstrip Lines," *IEEE Microwave and Guided Wave Lett.*, Vol. 8, No. 2, pp. 69-71, Feb. 1998.

[4] K. Agi, L.D. Moreland, E. Schamiloglu, M. Mojahedi and K.J. Malloy and E.R. Brown, "Photonic Crystals: A New Quasi-optical Component for High-Power Microwaves," *IEEE Trans. on Plasma Science, Sixth Special Issue on High Power Microwave Generation*, vol. 24, no.3, June 1996.

[5] E.R. Brown, C.D. Parker, and O.B. McMahon, "Effect of Surface Composition on the Radiation Properties from a Photonic-Crystal Planar-Dipole Antenna," *Appl. Phys. Lett.*, vol. 64, June 1994.

[6] M.M. Sigalas, R. Biswas, Q. Li, D. Crouch, W. Leung, R. Jacobs-Woodbury, B. Lough, S. Nielsen, S. McCalmont, G. Tuttle and K.-M. Ho, "Dipole Antennas on Photonic Bandgap Crystals – Experiment and Simulations," *Microwave and Opt. Tech. Lett.*, vol. 15, June 1997.

[7] M.P. Kessler, J.G. Maloney, B.L. Shirley and G. S. Smith, "Antenna Design with the Use of Photonic Band Gap Materials as All Dielectric Planar Reflectors," *Microwave and Opt. Tech. Lett.*, vol. 11, March 1996.

[8] H.Y.D. Yang, N.G. Alexopoulos and E. Yablonovitch, "Photonic Band-Gap Materials for High-Gain Printed Circuit Antennas," *IEEE Trans. on Ant. and Prop.*, vol. 45, no. 1, January 1997.

[9] H. Everitt, Special Issue on "Development and Applications of Materials Exhibiting Photonic Bandgaps," *J. Opt. Soc. Of Amer. B.*, vol. 10, no.2., Feb. 1993.

[10] K.S. Kunz and R.J. Leubbers, *The Finite Difference Time Domain Method for Electromagnetics* (CRC Press, Boca Raton, Florida, 1993).

[11] A. Taflove, *Computational Electromagnetics: The Finite-Difference Time-Domain Method* (Artech House, Norwood, MA, 1995).

[12] D.M. Pozar and D. H. Schaubert, *Microstrip Antenna: The Analysis and Design of Microstrip Antennas and Arrays* (IEEE Press, New York, 1995).

[13] XFDTD is a Registered Trademark of Remcom, Inc. (www.remcom.com).

[14] "The FDTD Method as Implemented in XFDTD," Remcom Inc. short course notes on XFDTD, University Park, PA, March 1998.

[15] H. Hertz, *Electric Waves* (Macmillan, London, 1893), p. 107.

[16] W. R. Hamilton, Proc. Roy. Irish Acad. **1**, (1839) pp. 267, 341.

[17] J. W. Strutt, and B. Rayleigh, *The theory of sound* (Dover, New York, 1945), p.475.

[18] L. Brillouin, *wave Propagation and Group Velocity* (Academic Press, New York, 1960).

[19] L. A. MacColl, Phys. Rev. **40**, 621 (1932).

[20] T. E. Hartman, J. Appl. Phys. **33**, 3427 (1962).

[21] T. K. Gaylord, G. N. Henderson, and E. N. Glytsis, J. Opt. Soc. Am. B **10**, 333 (1993).

[22] Th. Martin, and R. landauer, Phys. Rev. A **45**, 2611 (1992).
[23] R. Y. Chiao, P. G. Kwiat, and A. M. Steinberg, Physica **B 175**, 257 (1991).
[24] A. M. Steinberg, and R. Y. Chiao, Phys. Rev. A **49**, 3283 (1994).
[25] A. M. Steinberg, P. G. Kwiat, and R. Y. Chiao, Phys. Rev. Lett. **71**, 708 (1993).
[26] Ch. Spielmann, R. Szipöcs, A. Stingl, and F. Krausz, Phys. Rev. Lett. **73**, 2308 (1994).
[27] A. Ranfagni, D. Mugnai, P. Fabeni, and G. P. Pazzi, Appl. Phys. Lett. **58**, 774 (1991).
[28] A. Ranfagni, D. Mugnai, P. Fabeni, G. P. Pazzi, G. Naletto, and C. Sozzi, Physica **B 175**, 283 (1991).
[29] A. Ranfagni, P. Fabeni, G. P. Pazzi, and D. Mugnai, Phys. Rev. E **48**, 1453 (1993).
[30] A. Enders, and G. Nimtz, J. Phys. I France **2**, 1693 (1992).
[31] A. Enders, and G. Nimtz, Phys. Rev. B **47**, 9605 (1993).
[32] A. Enders, and G. Nimtz, Phys. Rev. E **48**, 632 (1993).
[33] A. Enders, and G. Nimtz, J. Phys. I France **3**, 1089 (1993).
[34] G. Nimtz, A. Enders, and H. Spieker, J. Phys. I France **4**, 565 (1994).
[35] M. V. Klein, and T. E. Furtak, *Optics* (John Wiley & Sons, New York, 1986), pp. 295-300.
[36] M. Born, and E. Wolf, *Principles of optics* (Pergamon, Oxford, 1970), p. 57.
[37] *Ibid*, pp. 66-70.
[38] J. P. Dowling, IEE P-Optoelectronics, Special issue on PBG **145**, (to be published).
[39] G. Strang, *Liner algebra and its applications* (Harcourt Brace Jovanovich, San Diego, 1988), pp. 254-260.
[40] *HP 8719D/8720D/8722D Network Analyzer User's Guide* (Hewlett Packard, 1997).
[41] *Network Analysis. Applying the HP 8510 TRL calibration for non-coaxial measurements* (Product Note 8510-8A).
[42] M. Mojahedi, E. Schamiloglu, K. Agi, and K. J. Malloy (unpublished).
[43] *Measuring Dielectric Constant with the HP 8510 Network Analyzer* (Product Note 8530-3).
[44] In the case of an infinite 1DPC, the wave vector in the gap is purely imaginary, and hence the associated phase is constant.
[45] The nominal value of these variables was obtained by averaging several measurements. For example, the average value of the spacer thickness after 16 measurements was 1.76 cm. The nominal values for the indices and thicknesses were: $n_i = 1.0$, $n_j = n_j^{'} - i\, n_j^{''} = 3.40 - i\, 0.002$, $d_i = 1.76$ cm, $d_j = 1.33$ cm.
[46] The fitting parameters for the case of N=2 were $d_i = 1.825$ cm, $d_j = 1.366$ cm, and $n_j^{'} = 3.288$, and the fitting parameters for the case of N=1 were: $d_j = 1.396$ cm, and $n_j^{'} = 3.245$. In all cases, $n_j^{''} = 0.002$.
[47] J. D. Jackson, *Classical Electrodynamics* (Wiley, New York, 1975), p. 302.
[48] Ref. [36], p.23.
[49] M. D. Crisp, Phys. Rev. A **4**, 2104 (1971).
[50] E. L. Bolda, R. Y. Chiao, and J. C. Garrison, Phys. Rev. A **48**, 3890 (1993).
[51] G. Diener, Phys. Lett. A **223**, 327 (1996).
[52] R. Y. Chiao, J. Boyce, and M. W. Mitchell, Appl. Phys. B **60**, 259 (1995).
[53] R. Y. Chiao, and A. M. Steinberg, Progress in Optics **37**, 345 (1997).

[54] M. Scalora, J. P. Dowling, A. S. Manka, C. M. Bowden, and J. W. Haus, Phys. Rev. A **52**, 726 (1995).